Microscopic study of ^{16}O + ^{16}O fusion

C. Simenel,[1] R. Keser,[2] A. S. Umar,[3] and V. E. Oberacker[3]

[1]*Department of Nuclear Physics, RSPE, Australian National University, Canberra, ACT 0200, Australia*
[2]*RTE University, Science and Arts Faculty, Department of Physics, 53100 Rize, Turkey*
[3]*Department of Physics and Astronomy, Vanderbilt University, Nashville, Tennessee 37235, USA*

We perform a study of ^{16}O + ^{16}O fusion at above and below the interaction barrier energies using three-dimensional time-dependent Hartree-Fock (TDHF) calculations at above-barrier energies and density-constrained TDHF calculations for the entire energy range. We discuss the variations of the experimental data at above the barrier energies. Calculations reasonably reproduce the observed energy-dependent broad oscillations in the fusion excitation functions. These oscillations result from overcoming L-dependent fusion barriers. The role of the coupling to low-lying octupole states is also discussed.

PACS number(s): 21.60.Jz, 24.10.−i, 25.70.Jj

I. INTRODUCTION

Collisions of light heavy ions constitute one of the most interesting areas of low-energy nuclear physics. Scattering of light systems seems to reveal the internal structure of the colliding nuclei as well as the structure of the composite system in a profound way. One of the manifestations of this interplay between structure and reactions is the observation of regular energy-dependent structures in most scattering cross sections for collision energies above the Coulomb barrier [1,2]. In conjunction with reaction theory, clustering models [3,4], mean-field studies of shape isomeric resonances and molecular formations [5–8], and adiabatic time-dependent Hartree-Fock (TDHF) calculations [9] of fusion barriers have been some of the microscopic approaches used to study phenomena associated with light systems.

Structures in fusion cross sections are possible experimental signatures of nuclear molecules [10,11]. However, structures in fusion excitation functions may also appear in light systems which are not necessarily due to the formation of nuclear molecules. Such structures or oscillations appear clearly in cross sections for the fusion of ^{12}C + ^{12}C [12], ^{12}C + ^{16}O [13], ^{16}O + ^{16}O [14–16], and ^{20}Ne + ^{20}Ne [17]. In particular, the discrete nature of angular momentum may reveal itself in fusion excitation functions as peaks associated with barriers for specific angular momenta [17–20].

In addition to the intriguing aspects mentioned above, sub-barrier fusion cross sections of light systems also carry a significance for astrophysical applications [21–23]. This need for fusion cross sections at extreme sub-Coulomb-barrier energies have led to the discussion of fusion hindrance for such systems [24,25]. Recently, Esbensen has provided a comprehensive coupled-channels study of the ^{16}O + ^{16}O fusion for the full energy regime [19]. Since most of the data [14–16,26–29] for the ^{16}O + ^{16}O system are more than a quarter of a century old, theoretical studies have been the main tool of recent investigations. As we will discuss below, large variations in the available fusion data at above-barrier energies have made such studies more difficult.

It is generally acknowledged that the TDHF method provides a useful foundation for a fully microscopic many-body theory of low-energy heavy-ion reactions [30,31]. This assumption is predicated in part on the results of fusion excitation calculations for light-mass systems and particular energy-angle correlation-function calculations for strongly damped heavy-mass collisions. Fusion of ^{16}O + ^{16}O at above-barrier energies was one of the primary testing systems for early TDHF calculations [32–37], primarily because ^{16}O is doubly magic and light systems were easier for computational reasons. The initial results showed reasonable agreement with higher energy (around 34 MeV) fusion data. However, this was mostly the result of the so-called fusion window anomaly, a nonzero lower angular momentum limit for fusion due to an unusual degree of transparency for central collisions. This central deep-inelastic region was not seen experimentally. Later it was shown that this was primarily due to an approximation made in the effective interaction, the absence of the spin-orbit term [38,39]. In these older TDHF calculations, axial symmetry was mostly assumed and lower order discretization techniques were used for numerical implementation. Noncentral impact parameters were often treated via the "rotating-frame approximation" [32,34]. Today, most TDHF codes employ higher order interpolation methods and operate on a fully three-dimensional lattice with no unphysical symmetry assumptions [40]. Naturally, three-dimensional calculations show a higher degree of dissipation in comparison to the two-dimensional counterparts due to an increased number of degrees of freedom sharing the available energy. In fact, modern TDHF calculations of fusion reactions have reached a good level of description both for light systems [40–43] and heavy systems where fusion hindrance is expected [31,44]. Predictions of reaction dynamics in actinide collisions have also been made recently [45,46].

Almost all TDHF calculations have been done using the Skyrme energy density functional (EDF) [47]. In addition to the omission of the spin-orbit term, earlier TDHF calculations also replaced some of the numerically difficult terms in the Skyrme interaction with a finite-range Yukawa form [48], without a new fit to the nuclear properties. Modern Skyrme forces have much improved fit properties to nuclear data that significantly reduce the variations among them for reproducing global nuclear properties [49,50]. Finally, it is well known

[51] that the Skyrme energy density functional also contains time-odd terms which depend on the spin density, spin kinetic energy density, and the full spin-current pseudotensor. The time-odd terms vanish for static calculations of even-even nuclei but they should be present for time-dependent calculations to maintain the Galilean invariance of the collision process [52]. The Skyrme energy density functional does remain time-reversal invariant as all the time-odd terms enter in quadratic form or as linear byproducts. Many of these terms have not been included in older TDHF calculations because of numerical difficulty. The latest generation of TDHF codes [40,53] used in this study contain all of these time-odd terms.

Fusion at sub-barrier energies is a very challenging problem for nuclear theory. In particular, it may be extremely sensitive to the internal structure of the collision partners, such as their low-lying collective modes [54]. Currently, there is no implementation based on a true quantum many-body theory of barrier tunneling. In all sub-barrier fusion calculations one assumes the existence of an ion-ion potential $V(R)$ which depends on the internuclear distance R. While phenomenological heavy-ion potentials (e.g., Woods-Saxon or double-folding) provide a useful starting point for the analysis of fusion data, it is desirable to use a quantum many-body approach which properly describes the underlying nuclear shell structure of the reaction system. During the past several years, we have developed the density constrained time-dependent Hartree-Fock (DC-TDHF) method for calculating heavy-ion potentials $V(R)$ [55–59] which incorporate all of the dynamical entrance channel effects such as neck formation, particle exchange, internal excitations, and deformation effects [60].

In this paper we carry out TDHF calculations of fusion cross sections for the ^{16}O + ^{16}O system without making any of the approximations used in earlier calculations. In the next section we discuss the experimental fusion data. This is followed by above-barrier fusion calculations directly using TDHF. Transfer channels and inelastic excitation of octupole states are then discussed. Finally, both sub-barrier and above-barrier fusion cross sections are calculated using the DC-TDHF approach of obtaining potential barriers from the TDHF time evolution.

II. EXPERIMENTAL DATA

During the late 1970s and early 1980s the observed structures in fusion excitation functions for light-A systems prompted a flurry of experiments measuring fusion cross sections for these systems [1]. Figure 1 shows a selected set of experimental fusion cross sections for the ^{16}O + ^{16}O system. The cross section at higher energies is characterized by broad energy-dependent oscillations.

Unlike heavy-mass systems, for the collisions of light nuclei at bombarding energies well above the Coulomb barrier the thermalization of the available energy is much slower, thus resulting in collective excitations of the composite system with a large number of breakup channels. Consequently, the de-excitation mechanism of the compound system is primarily through the emission of light-A products as opposed to
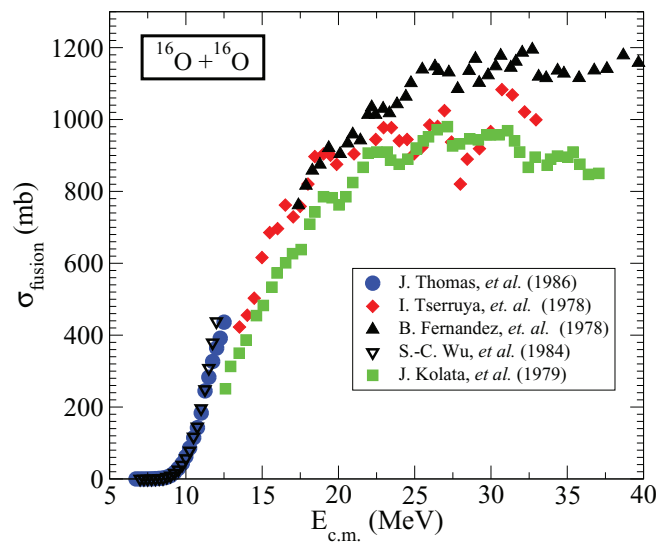

FIG. 1. (Color online) Experimental data for the ^{16}O + ^{16}O fusion excitation functions plotted on a linear scale.

emission of primary γ rays. The fission mode is assumed to be negligible for light systems. Broadly, the experimental approach to measuring above-barrier fusion cross sections for light-mass systems falls into three categories. The first method involves the detection of particle yields originating from fusion products and is the method used in the earliest experiments [61], the second method relies on the detection of the de-excitation γ rays from nuclides produced as evaporation residues (with Kolata *et al.* [16] detecting 12 nuclides), and the last method uses a time-of-flight technique to identify evaporation residues (with Fernandez *et al.* [14] detecting fragments with $A > 20$). Tserruya *et al.* [15] use both the time-of-flight data and a ΔE-E telescope to identify all products with $Z > 10$ or $A > 20$ as evaporation residue. Each one of these methods has advantages and disadvantages. In addition to their dependence on the detection system and associated corrections, techniques to identify γ rays from evaporation residue fail to account for transitions to the ground state and residues formed without γ emission. Moreover, high-energy γ rays cannot be used to identify nuclei. The barrier top and sub-barrier fusion data of Wu and Barnes [26] and Thomas and co-workers [27,28] are consistent with each other. In these two experiments a lot of attention was paid to degradation (evaporation) of the target by using gold-plated targets and cross-checking the target thickness with Rutherford Coulomb back-scattering measurements. Among the higher energy experiments, Fernandez *et al.* use elastic scattering measurements at the beginning and end of an experimental run to assure that target thicknesses have not changed. Changing thickness may result in a change in normalization of the cross sections. Unfortunately, their data do not extend to lower energies to compare with the lower energy data. Wu and Barnes undertake a comparison of their results with other experiments at $E_{\rm c.m.} = 12$ MeV and argue that if Kolata *et al.* data at this energy are corrected by their summing and branching ratio factor the two results are in much closer agreement (438 versus 481 mb). Somewhat smaller differences have been found by

Kuronen *et al.* [29], who have measured the fusion cross sections between 8 and 14 MeV and compared their results with the Wu and Barnes and the Thomas data and some of the older data. Resolution of these differences at all energies is highly desirable.

III. TDHF STUDIES OF ^{16}O + ^{16}O FUSION

A. Above-barrier TDHF calculations

In this section we present results for ^{16}O + ^{16}O fusion by directly using the TDHF3D code [53] at energies above the Coulomb barrier. The TDHF equation

$$i\hbar \frac{d\rho}{dt} = [h[\rho], \rho], \qquad (1)$$

where ρ is the one-body density matrix of the independent particle system, and $h[\rho]$ is the self-consistent single-particle HF Hamiltonian, is solved iteratively with a time step $\Delta t = 1.5 \times 10^{-24}$ s. The wave function is developed on a three-dimensional grid of $56 \times 28 \times 28 \Delta x^3$, where the mesh grid is $\Delta x = 0.8$ fm, and with a plane of symmetry (the collision plane). More numerical details can be found in Ref. [31].

The interpretation of fusion reactions in terms of semiclassical trajectories obtained from the TDHF theory exhibits the best agreement with experiment for the lightest systems, since here fusion comprises almost the entire reaction cross section. Traditionally, the fusion cross section is given by

$$\sigma_{fus}(E_{\text{c.m.}}) = \frac{\pi\hbar^2}{2\mu E_{\text{c.m.}}} \sum_{L=0}^{\infty} (2L+1) P_{fus}(L, E_{\text{c.m.}}), \qquad (2)$$

where μ is the reduced mass of the system, and $P_{fus}(L, E_{\text{c.m.}})$ is the fusion probability for the partial wave with orbital angular momentum L at the center-of-mass energy $E_{\text{c.m.}}$. Due to the restriction to a single mean field, TDHF calculations do not include sub-barrier tunneling of the many-body wave function, i.e., $P_{fus}^{TDHF} = 0$ or 1. As a result, the fusion cross section can be estimated with the quantum sharp cutoff formula [62]

$$\sigma_{fus}(E_{\text{c.m.}}) = \frac{\pi\hbar^2}{2\mu E_{\text{c.m.}}} \sum_{L=0}^{L_{\max}(E_{\text{c.m.}})} (2L+1)$$

$$= \frac{\pi\hbar^2}{2\mu E_{\text{c.m.}}} [L_{\max}(E_{\text{c.m.}}) + 1]^2, \qquad (3)$$

where $L_{\max}(E_{\text{c.m.}})$ is the maximum angular momentum at which fusion occurs at $E_{\text{c.m.}}$. For symmetric systems with 0^+ ground states, fusion can only occur for even values of the angular momentum. The cross section with the sharp cutoff formula then reads

$$\sigma_{fus}(E_{\text{c.m.}}) = \frac{\pi\hbar^2}{2\mu E_{\text{c.m.}}} [L_{\max}(L_{\max} + 3) + 2]. \qquad (4)$$

We have computed fusion cross sections for the ^{16}O + ^{16}O system as a function of energy with the SLy4d Skyrme energy density functional [53]. At each center-of-mass energy, a series of runs was performed to pinpoint the ending of fusion or beginning of the deep-inelastic regime, thus yielding the $L_{\max}$ value. The results of these calculations expressed via Eq. (4)
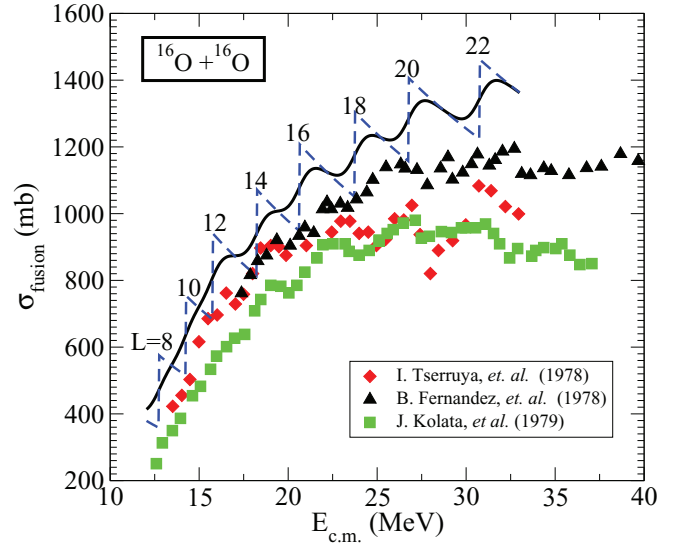

FIG. 2. (Color online) Above-barrier fusion cross sections as a function of center-of-mass energy in ^{16}O + ^{16}O obtained with TDHF calculations. The cross sections are computed with the sharp cutoff formula (dashed line) and using Eq. (5) for the barrier penetration probabilities (solid line). The numbers indicate the position of the barriers $B(L)$.

are shown in Fig. 2 with a dashed line. The sharp increases of the fusion cross sections at the positions of the angular-momentum-dependent barriers $B(L)$ are due to the fact that fusion penetration probabilities are either 0 or 1 at the TDHF level.

The sharp edges observed in Fig. 2 can be smoothed by considering tunneling in an approximate way. As a first approximation, one can estimate the barrier penetration probability according to the Hill-Wheeler formula [63] with a Fermi function:

$$P_{fus}(L, E_{\text{c.m.}}) \simeq \frac{e^{x_L}}{1 + e^{x_L}}, \qquad (5)$$

with $x_L = [E - B(L)]/\varepsilon$. Choosing the decay constant $\varepsilon = 0.4$ [20], one gets the fusion cross sections represented by the solid line in Fig. 2.

An overall overestimation of the experimental data of Fernandez *et al.* [14] by $\sim 16\%$ is obtained. It is interesting to note that the same factor was obtained for the ^{16}O + ^{208}Pb system, while the predicted position of the barrier is in excellent agreement with experiment [31]. Note that this systematic discrepancy remains small, in particular given the fact that the TDHF calculations have no input coming from reaction mechanisms.

Oscillations for $E_{\text{c.m.}} > 16$ MeV are clearly visible and due to L-dependent barriers with $L \geqslant 12\hbar$. Note that these oscillations would be less visible for asymmetric systems because all integer values of L are possible. In addition, the observation of these oscillations is limited to light systems up to, e.g., ^{28}Si + ^{28}Si [20,64]. For heavier systems, the oscillations are indeed expected to be smeared out as the coupling to many reaction channels sets in [20].

B. Role of transfer at sub-barrier energies

In order to get a deeper insight into the dynamical mechanisms at play in the fusion process, the TDHF approach can also be used to estimate the importance of other channels around the barrier. Let us first investigate the particle transfer at sub-barrier energies. Indeed, transfer channels could be a doorway to dissipation and, then, reduce the fusion probability [65]. The TDHF approach has been used to investigate quasielastic transfer reactions in heavy-ion collisions in recent works [65–71]. The proton and neutron transfer probabilities have been computed in ^{16}O + ^{16}O at $E_{c.m.} = 10$ MeV, i.e., just below the barrier, using the particle number projection technique developed in Ref. [68]. The resulting probabilities are extremely small, i.e., $p_{1n} \sim p_{1p} \sim 3 \times 10^{-6}$, which is at the level of the numerical noise. These results have been confirmed in beyond-TDHF calculations where fluctuations at the time-dependent random-phase approximation (RPA) level are included (see Refs. [31,72,73] for details of the technique). The fact that the transfer probabilities are so small in this reaction is essentially due to the large negative Q values for these channels. Note that the single-particle wave functions belonging initially to one nucleus can still be partially transferred to the other fragment [31]. However, this process, being symmetric, does not change the fragment particle number distributions. Only transfer to a single-particle state above the Fermi level, which is energetically unfavored, would induce fluctuations of the particle number probabilities in the fragments. Note that in these calculations possible correlations which could enhance, e.g., nucleon pair transfer are neglected [65]. Beyond TDHF calculations including such correlations should be considered to treat transfer of paired nucleons [74]. However, pair transfer is unlikely to exceed the transfer of one independent particle. We then conclude that the sub-barrier fusion in ^{16}O + ^{16}O is not affected by transfer channels.

C. Coupling to low-lying octupole states

In addition to quasielastic transfer, inelastic excitation of low-lying collective states is also known to strongly affect fusion around and below the barrier [54]. Both the coupled-channel approach [75] and TDHF calculations have been used to study the coupling between fusion and rotational motion [56,76] and between fusion and vibrational modes [41,77,78]. In the present case, the coupling of the relative motion to the 3_1^- octupole phonon in ^{16}O at $E_{3_1^-} = 6.129$ MeV [79] may induce a global shift of the barrier to lower energies [80]. The expectation value of the octupole moment can be computed from the local part of the one-body density using

$$Q_3(t) = \sqrt{\frac{7}{16\pi}} \int d^3r \rho(\mathbf{r})[2\bar{x}^3 - 3\bar{x}(\bar{y}^2 + \bar{z}^2)], \quad (6)$$

where $\bar{\xi} = \xi - \xi_{c.m.}$. Because the center of the numerical box in the TDHF calculations is located at $x = y = z = 0$, the octupole moment in one fragment of a central symmetric collision can be obtained by considering the integral in the $x > 0$ region in Eq. (6) and using the coordinates of the center of mass of the matter distributed in the same region. The
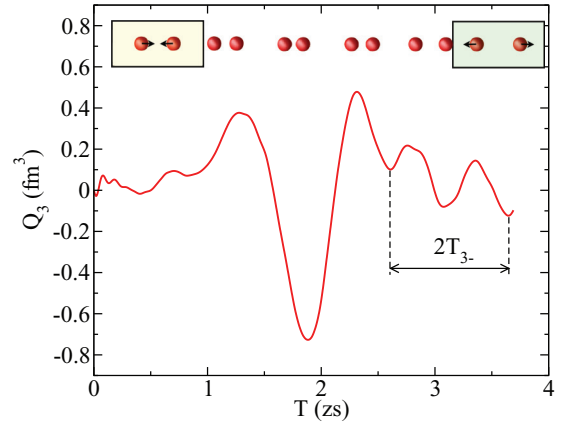

FIG. 3. (Color online) Time evolution of the octupole moment of the fragment in $x > 0$ in an ^{16}O + ^{16}O collision at $E_{c.m.} = 10$ MeV. The arrow indicates the time interval $2T_{3^-}$ during which two oscillations of the octupole moment occur. The snapshots show the isodensity at half the saturation density, $\rho_0/2 = 0.08$ fm^{-3}, at $T = 0.6, 1.2, 1.8, 2.4, 3.0,$ and 3.6 zs. The numerical box is shown for the first and last snapshots.

evolution of $Q_3(t)$ of the fragment in the $x > 0$ region in an ^{16}O + ^{16}O collision at $E_{c.m.} = 10$ MeV is shown in Fig. 3. Snapshots of the density are also shown at different times. The increase of Q_3 in the approach phase can be interpreted as an effect of Coulomb repulsion inducing an octupole polarization of the fragments. At short distances between the fragments, the nuclear interaction reverses this polarization and tends to form a neck between the fragments. After reseparation occurs, the octupole moment clearly oscillates in the exit channel. The period of this oscillation can be determined from Fig. 3. As a result, we get $T_{3^-} \simeq 0.56$ zs. In the harmonic picture, this oscillation is associated with a vibrational mode at $E_{3^-} = \hbar \frac{2\pi}{T_{3^-}} \simeq 7.4$ MeV, which is slightly higher than the experimental value of the 3_1^- state.

To get a clear assignment of this vibration to the 3_1^- phonon, the spectrum of 3^- states has been determined at the RPA level using the same TDHF code with the linear response theory (see Refs. [31,81] for similar calculations of bound states and Refs. [82–88] for unbound states). The TDHF response to an octupole boost $e^{-i\varepsilon \hat{Q}_3}$ applied on the ^{16}O Hartree-Fock ground state has been computed. Note that the initial state is spherical and $Q_3(0) = 0$. The boost velocity ε is chosen small enough to be in the linear regime, i.e., $Q_3(t) \propto \varepsilon$. The time evolution of $Q_3(t)$ is shown in the inset of Fig. 4. The octupole strength distribution $S_{3^-}(E)$ is determined from $Q_3(t)$ according to

$$S_{3^-}(E) = \frac{-1}{\pi \hbar \varepsilon} \int_0^\infty dt\, Q_3(t) \sin(Et/\hbar) \quad (7)$$

and is shown in Fig. 4. A large peak at $E_{3^-} \simeq 7.67$ MeV and exhausting $\sim 11.2\%$ of the energy weighted sum rule (EWSR) can be seen. Both the energy and the strength of this peak are of the same order as the 3_1^- experimental state (respectively, $E_{3_1^-} = 6.129$ MeV and $13.1\% \pm 0.6\%$ of the EWSR [79]). Its energy is close to the energy extracted from the time evolution of the octupole moment of the fragment in Fig. 3. The peak at 7.67 MeV in Fig. 4 is associated with the first phonon of
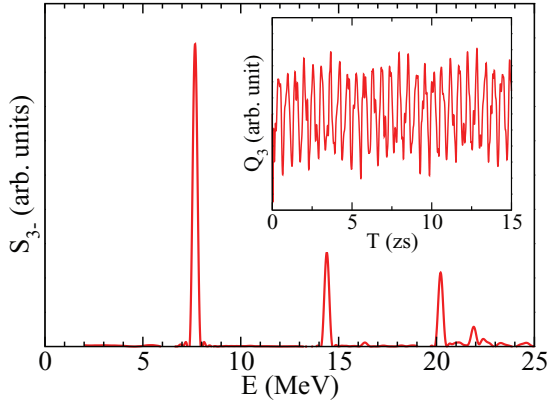
FIG. 4. (Color online) Strength function of the octupole moment in ^{16}O obtained from the time evolution of the octupole moment in the linear regime shown in the inset.

the low-lying octupole vibration in ^{16}O, and it clearly gives rise to the oscillation observed in the exit channel in Fig. 3. Note that other peaks are seen in Fig. 4. Several candidates in the spectrum of 3^- states in ^{16}O could be associated with these peaks. However, their effect on the fusion process is expected to be minor compared to the coupling to the 3_1^- phonon, due to their lower strength and larger excitation energy than the 3_1^- state [80].

The effect of low-lying collective excitations on fusion cross sections is usually studied with the coupled-channel approach [75]. In principle, a microscopic approach such as TDHF could be used to determine the parameters entering coupled-channel calculations. This will be the purpose of a future work. Here, the effect of the coupling to the 3_1^- state on the fusion process is illustrated on Fig. 5 with standard
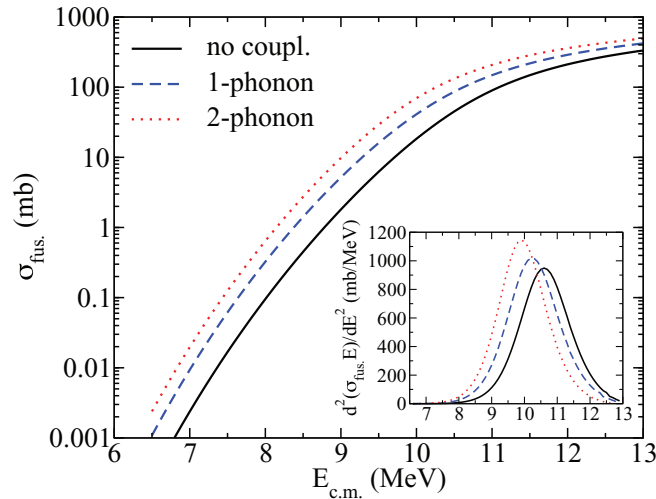

FIG. 5. (Color online) Fusion cross sections in the ^{16}O + ^{16}O system calculated with the CCFULL code with no coupling (solid line), including the coupling to the 3_1^- state of one nucleus (dashed line), and including the coupling to the 3_1^- state of both nuclei (dotted line). The inset shows the estimate of the barrier distribution from the second derivative of $\sigma_{fus} E$. The parameters of the Woods-Saxon nucleus-nucleus potential and of the coupling are described in the text.

coupled-channel calculations using the CCFULL code [89]. The nucleus-nucleus potential is a Woods-Saxon potential with a depth $V_0 = -65.4$ MeV, a diffuseness $a = 0.60$ fm, and a radius parameter $r_0 = 1.0625$. These parameters have been fitted to reproduce the Sao Paulo potential [90] for this system. The barrier height resulting from this bare potential is $V_B \simeq 10.7$ MeV. The deformation parameter for the nuclear and Coulomb coupling to the 3_1^- is taken to be $\beta_3 = 0.733$ [80] with the experimental energy $E_{3_1^-} = 6.129$ MeV. We see in Fig. 5 that the main effect of the coupling is a global lowering of the barrier by ~ 0.3 MeV per phonon. When the two phonons are included (one per nucleus), this leads to an enhancement of the sub-barrier fusion by about one order of magnitude. To conclude, whereas transfer channels can be neglected, we see that the inelastic excitation of low-lying vibrational modes is playing a major role in ^{16}O + ^{16}O fusion.

IV. DC-TDHF STUDIES OF ^{16}O + ^{16}O FUSION

The concept of using density as a constraint for calculating collective states from TDHF time evolution was first introduced in Ref. [91] and was used in calculating collective energy surfaces in connection with nuclear molecular resonances in Ref. [6]. However, its utilization to calculate microscopic heavy-ion potentials had not been realized until recently [55]. In recent years the DC-TDHF method has been applied to calculate fusion barriers and corresponding cross sections for over twenty systems.

In this approach we assume that a collective state of the system is characterized only by the instantaneous TDHF neutron and proton densities. The lowest static collective energy corresponding to these densities can be calculated by solving the density-constrained density-functional problem

$$E_{DC}(t) = \min_{\rho_n, \rho_p} \left\{ E[\rho_n, \rho_p] + \int d\mathbf{r}\, v_n(\mathbf{r}) \left[\rho_n(\mathbf{r}) - \rho_n^{tdhf}(\mathbf{r}, t) \right] \right.$$
$$\left. + \int d\mathbf{r}\, v_p(\mathbf{r}) \left[\rho_p(\mathbf{r}) - \rho_p^{tdhf}(\mathbf{r}, t) \right] \right\}, \qquad (8)$$

where $E[\rho_n, \rho_p]$ is the same density functional used in the TDHF (Skyrme functional) formulation and additional dependencies have been omitted for notational simplicity; the quantities $v_{n,p}(\mathbf{r})$ are the Lagrange multipliers, which represent external fields that constrain the densities during the minimization procedure. Equation (8) is equivalent to solving static Hartree-Fock equations subject to the constraints on neutron and proton densities to remain equal to the instantaneous TDHF densities while minimizing the energy.

In terms of this state one can write the collective energy as

$$E_{coll}(t) = E_{kin}(\rho(t), \mathbf{j}(t)) + E_{DC}(\rho(\mathbf{r}, t)), \qquad (9)$$

where the collective kinetic energy E_{kin} is defined as

$$E_{kin} \approx \frac{m}{2} \sum_q \int d^3 r\, \mathbf{j}_q^2(t) / \rho_q(t), \qquad (10)$$

with index q being the isospin index for neutrons and protons ($q = n, p$).

This collective energy differs from the conserved TDHF energy only by the amount of internal excitation present in the TDHF state, namely,

$$E^*(t) = E_{\text{TDHF}} - E_{\text{coll}}(t). \quad (11)$$

From Eq. (9) it is clear that the density-constrained energy E_{DC} plays the role of a collective potential. In fact this is exactly the case except for the fact that it contains the binding energies of the two colliding nuclei. One can thus define the ion-ion potential as [55]

$$V = E_{\text{DC}}(\rho(\mathbf{r}, t)) - E_{A_1} - E_{A_2}, \quad (12)$$

where E_{A_1} and E_{A_2} are the binding energies of two nuclei obtained from a static Hartree-Fock calculation with the same effective interaction. For describing a collision of two nuclei one can label the above potential with ion-ion separation distance $R(t)$ obtained during the TDHF time evolution. This ion-ion potential $V(R)$ is asymptotically correct since at large initial separations it exactly reproduces $V_{\text{Coulomb}}(R_{\text{max}})$, where $R_{\text{max}} = 14.5$ fm is the initial distance between the nuclei in the DC-TDHF calculations. In addition to the ion-ion potential, it is also possible to obtain coordinate-dependent mass parameters. One can compute the "effective mass" $M(R)$ using the conservation of energy at the zero impact parameter:

$$M(R) = \frac{2[E_{\text{c.m.}} - V(R)]}{\dot{R}^2}, \quad (13)$$

where the collective velocity $\dot{R}$ is directly obtained from the TDHF evolution and the potential $V(R)$ from the density constraint calculations. This coordinate-dependent mass can be exactly incorporated into the potential $V(R)$ by using a point transformation [57].

For the $^{16}\text{O} + ^{16}\text{O}$ system we have shown [23] excellent agreement between our calculations and the low-energy sub-barrier data from Refs. [27,28]. We now extend this work to higher energies to see how our results compare with the available data. In Fig. 6 we show the calculated DC-TDHF ion-ion potential for the $^{16}\text{O} + ^{16}\text{O}$ system evaluated at a TDHF c.m. energy of 12 MeV. For comparison we also display the corresponding point-Coulomb potential. The potential barrier has a height of 10.05 MeV. For this system there is practically no dependence of the DC-TDHF barrier on the c.m. energy even if we increase the energy as much as five times the barrier height. This is generally true for light compact systems whereas for heavy systems a strong energy dependence of DC-TDHF potentials is observed [58].

Figure 7 shows the fusion cross sections corresponding to the DC-TDHF barrier shown in Fig. 6 (black solid curve) compared with the experimental data on a linear scale. The inset shows a logarithmic plot of the low-energy fusion cross sections, which are in excellent agreement with the experimental data [27,28]. It is interesting to note that the gross oscillations in the cross section at higher energies are correctly reproduced in our calculations. This is simply due to opening of new L channels as we increase the collision energy. Individual contributions to the cross section from higher L values are also shown on the lower part of the plot. Cross sections are calculated by directly integrating the Schrödinger
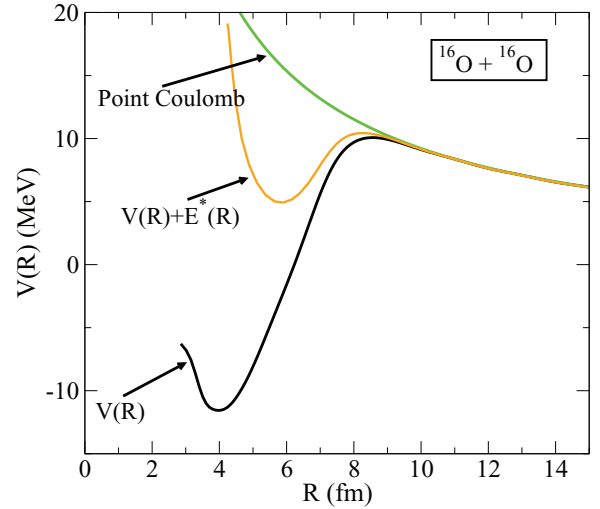

FIG. 6. (Color online) DC-TDHF ion-ion interaction potential for $^{16}\text{O} + ^{16}\text{O}$ obtained from TDHF calculations at $E_{\text{c.m.}} = 12$ MeV (black curve). Shown also is a potential which incorporates the excitation energy at $E_{\text{c.m.}} = 20$ MeV (orange curve), as well as the corresponding point-Coulomb potential (green curve).

equation

$$\left[\frac{-\hbar^2}{2\mu} \frac{d^2}{dR^2} + \frac{\hbar^2 \ell(\ell+1)}{2\mu R^2} + V(R) - E_{\text{c.m.}} \right] \psi_\ell(R) = 0, \quad (14)$$

using the well-established incoming wave boundary condition (IWBC) method [92] to obtain the barrier penetrabilities $P_{fus}(L, E_{\text{c.m.}})$ which determine the total fusion cross section [Eq. (2)]. We observe that, while the calculated cross sections are in excellent agreement with the data of Fernandez *et al.* [14], they are higher by as much as 25% than the lowest
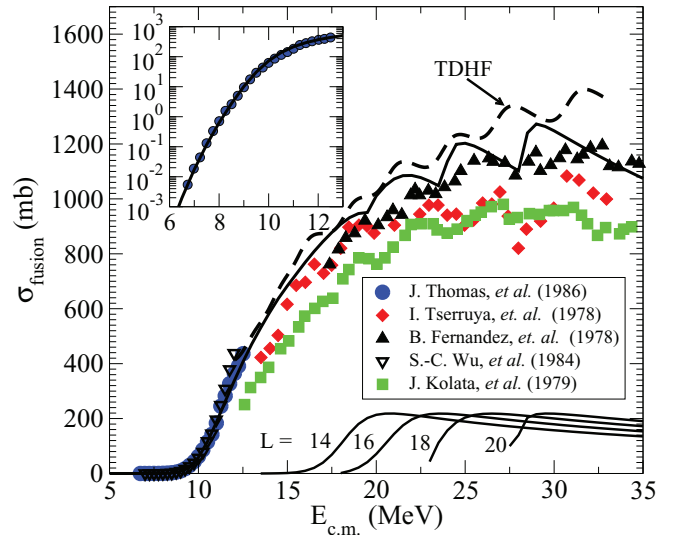

FIG. 7. (Color online) Fusion cross sections for $^{16}\text{O} + ^{16}\text{O}$ obtained from the DC-TDHF potential shown in Fig. 6 (black curve, calculated at $E_{\text{c.m.}} = 12$ MeV) compared with the TDHF calculations (dashed line) and with the experimental data. The lower curves show the contributions arising from the opening of new orbital angular momentum channels.

data points at $E_{\text{c.m.}} = 30$ MeV. However, one should keep in mind that the DC-TDHF potential was obtained by using a parameter-free microscopic theory.

The TDHF results of Fig. 2 have also been reported on Fig. 7 (dashed line). Although a good agreement with the DC-TDHF results is obtained at energies $E < 25$ MeV, the TDHF fusion cross sections are larger at higher energies. Detailed examination shows that this discrepancy is due to the earlier closing of the $L = 20$ window and the total absence of the $L = 22$ partial wave in the potential model calculations of the DC-TDHF formulation.

In the DC-TDHF formulation only the dynamical density evolution for the central collision is used in the calculation of the potential. Then the cross sections are determined using the isocentrifugal approximation. This is naturally an approximation to the full many-body calculation but seems to be a very good approximation at lower energies and allows the calculation of sub-barrier cross sections, where only small angular momenta L contribute. At the higher energies discussed in this paper (up to three times the barrier height), the fusion cross section is determined by larger values of the critical angular momentum. The smaller potential pocket at high L may lead to a higher sensitivity of the fusion cross section to the details of the potential. The observed discrepancy would indicate a breakdown of the isocentrifugal approximation, meaning that the TDHF potential at high L is not exactly the one at $L = 0$ plus a centrifugal potential. Naturally, direct TDHF calculations contain all of the dynamics and therefore should be more reliable at these energies.

The reactions of light systems at high energies (two to four times the barrier height) is complicated both experimentally and theoretically due to the presence of many breakup channels and excitations. We expect the TDHF results to yield a higher fusion cross section since many of the breakup channels are not naturally available in TDHF and they will appear as fusion. However, a closer investigation of the TDHF dynamics and the microscopically calculated excitation energy clearly indicates
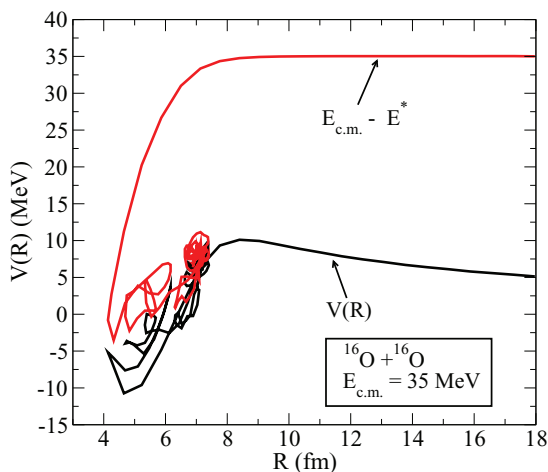
that a significant portion of the collective kinetic energy is not equilibrated. In Fig. 8 we show the long-time evolution of the DC-TDHF potential $V(R)$ together with the quantity $E_{\text{c.m.}} - E^*$ calculated at the TDHF energy $E_{\text{c.m.}} = 35$ MeV. We see that after the system traverses through the first potential minimum it starts to rise and go through successive higher minima and finally settles almost near the top of the entrance channel barrier. This is perhaps more clearly seen through the evolution of $E_{\text{c.m.}} - E^*$, which is some measure of dissipation. This behavior occurs because the excitation energy, E^*, is not distributed in an irreversible fashion but a certain fraction of it seems to be reversible, going into collective modes. In a fully quantal calculation this may partially lead to a breakup channel. The situation for the collision at $E_{\text{c.m.}} = 12$ MeV is very different. In this case the system settles close to the first barrier minimum.

V. CONCLUSIONS

A microscopic study of the ^{16}O + ^{16}O fusion reaction has been performed. Available experimental data sets above the barrier clearly disagree with each other. Calculations with the TDHF and the DC-TDHF methods are in better agreement with the data exhibiting the largest cross sections. The oscillations of the cross sections are interpreted as an effect of overcoming angular-momentum-dependent barriers. The sub-barrier cross sections are very well reproduced by the DC-TDHF calculations.

The DC-TDHF method has also been used to investigate the dissipative mechanisms. The latter rapidly set in inside the barrier, converting the kinetic energy of the relative motion into excitation energy of the fragments. In central collisions slightly above the barrier the system then settles close to the first barrier minimum. In contrast, well above the barrier the system settles near the top of the entrance channel barrier into a dinuclear configuration, possibly leading to a breakup channel.

The effect of coupling to other channels has been studied. Although the transfer reactions at sub-barrier energies are shown to be negligible, an oscillation of the octupole moment of the fragment in the exit channel indicates a coupling between the relative motion and the 3_1^- states in ^{16}O. Coupled-channel calculations show that this coupling shifts the barrier to lower energy, increasing the sub-barrier fusion cross section by about one order of magnitude.

Due to its small number of constituents, and to the magic nature of the collision partners, the ^{16}O + ^{16}O system is an ideal benchmark for low-energy reaction theory. Future theoretical models able to treat in a fully microscopic manner the reaction mechanisms from deep sub-barrier energies to well above the barrier should be tested on this system. However, reliable experimental data above the barrier are highly desirable.

FIG. 8. (Color online) Long-time evolution of the ion-ion potential, $V(R)$, and the excitation energy, $E_{\text{c.m.}} - E^*$, for the head-on collision of the ^{16}O + ^{16}O system at a collision energy of 35 MeV as a function of the ion-ion distance R.

[1] K. A. Erb and D. A. Bromley, in *Treatise on Heavy Ion Science*, edited by D. A. Bromley (Plenum, New York, 1985), Vol. 3, pp. 201.

[2] J. R. Birkelund, L. E. Tubbs, J. R. Huizenga, J. N. De, and D. Sperber, Phys. Rep. **56**, 107 (1979).

[3] W. von Oertzen, M. Freer, and Y. Kanada-En'yo, Phys. Rep. **432**, 43 (2006).

[4] N. Itagaki, W. von Oertzen, and S. Okabe, Phys. Rev. C **74**, 067304 (2006).

[5] R. R. Betts and A. H. Wuosmaa, Rep. Prog. Phys. **60**, 819 (1997).

[6] A. S. Umar, M. R. Strayer, R. Y. Cusson, P.-G. Reinhard, and D. A. Bromley, Phys. Rev. C **32**, 172 (1985).

[7] A. S. Umar and M. R. Strayer, Phys. Lett. B **171**, 353 (1986).

[8] C. Simenel, in *Clusters in Nuclei*, Vol. 3, Lecture Notes in Physics Vol. 875, edited by C. Beck (Springer, New York, 2013), pp. 95–145.

[9] K. Goeke, F. Grümmer, and P.-G. Reinhard, Ann. Phys. (NY) **150**, 504 (1983).

[10] E. C. Schloemer, M. Gai, J. F. Ennis, M. Ruscev, B. Shivakumar, S. M. Sterbenz, N. Tsoupas, and D. A. Bromley, Phys. Rev. Lett. **51**, 881 (1983).

[11] D. Lebhertz *et al.*, Phys. Rev. C **85**, 034333 (2012).

[12] P. Sperr, T. H. Braid, Y. Eisen, D. G. Kovar, F. W. Prosser, J. P. Schiffer, S. L. Tabor, and S. Vigdor, Phys. Rev. Lett. **37**, 321 (1976).

[13] P. Sperr, S. Vigdor, Y. Eisen, W. Henning, D. G. Kovar, T. R. Ophel, and B. Zeidman, Phys. Rev. Lett. **36**, 405 (1976).

[14] B. Fernandez, C. Gaarde, J. S. Larsen, S. Pontoppidan, and F. Videbaek, Nucl. Phys. A **306**, 259 (1978).

[15] I. Tserruya, Y. Eisen, D. Pelte, A. Gavron, H. Oeschler, D. Berndt, and H. L. Harney, Phys. Rev. C **18**, 1688 (1978).

[16] J. J. Kolata, R. M. Freeman, F. Haas, B. Heusch, and A. Gallmann, Phys. Rev. C **19**, 2237 (1979)

[17] N. Poffe, N. Rowley, and R. Lindsay, Nucl. Phys. A **410**, 498 (1983).

[18] R. Vandenbosch, Phys. Lett. B **87**, 183 (1979).

[19] H. Esbensen, Phys. Rev. C **77**, 054608 (2008).

[20] H. Esbensen, Phys. Rev. C **85**, 064611 (2012).

[21] L. R. Gasques, L. C. Chamon, D. Pereira, M. A. G. Alvarez, E. S. Rossi, C. P. Silva, and B. V. Carlson, Phys. Rev. C **69**, 034603 (2004).

[22] L. R. Gasques, A. V. Afanasjev, M. Beard, J. Lubian, T. Neff, M. Wiescher, and D. G. Yakovlev, Phys. Rev. C **76**, 045802 (2007).

[23] A. S. Umar, V. E. Oberacker, and C. J. Horowitz, Phys. Rev. C **85**, 055801 (2012).

[24] C. L. Jiang, K. E. Rehm, B. B. Back, and R. V. F. Janssens, Phys. Rev. C **75**, 015803 (2007).

[25] M. Dasgupta, D. J. Hinde, A. Diaz-Torres, B. Bouriquet, Catherine I. Low, G. J. Milburn, and J. O. Newton, Phys. Rev. Lett. **99**, 192701 (2007).

[26] S.-C. Wu and C. S. Barnes, Nucl. Phys. A **422**, 373 (1984).

[27] J. Thomas, Y. T. Chen, S. Hinds, K. Langanke, D. Meredith, M. Olson, and C. A. Barnes, Phys. Rev. C **31**, 1980 (1985).

[28] J. Thomas, Y. T. Chen, S. Hinds, D. Meredith, and M. Olson, Phys. Rev. C **33**, 1679 (1986).

[29] A. Kuronen, J. Keinonen, and P. Tikkanen, Phys. Rev. C **35**, 591 (1987).

[30] J. W. Negele, Rev. Mod. Phys. **54**, 913 (1982).

[31] C. Simenel, Eur. Phys. J. A **48**, 152 (2012).

[32] S. E. Koonin, Phys. Lett. B **61**, 227 (1976).

[33] R. Y. Cusson, R. K. Smith, and J. A. Maruhn, Phys. Rev. Lett. **36**, 1166 (1976).

[34] S. E. Koonin, K. T. R. Davies, V. Maruhn-Rezwani, H. Feldmeier, S. J. Krieger, and J. W. Negele, Phys. Rev. C **15**, 1359 (1977).

[35] H. Flocard, S. E. Koonin, and M. S. Weiss, Phys. Rev. C **17**, 1682 (1978).

[36] P. Bonche, B. Grammaticos, and S. E. Koonin, Phys. Rev. C **17**, 1700 (1978).

[37] K. T. R. Davies, H. T. Feldmeier, H. Flocard, and M. S. Weiss, Phys. Rev. C **18**, 2631 (1978).

[38] A. S. Umar, M. R. Strayer, and P.-G. Reinhard, Phys. Rev. Lett. **56**, 2793 (1986).

[39] P.-G. Reinhard, A. S. Umar, K. T. R. Davies, M. R. Strayer, and S.-J. Lee, Phys. Rev. C **37**, 1026 (1988).

[40] A. S. Umar and V. E. Oberacker, Phys. Rev. C **73**, 054607 (2006).

[41] C. Simenel, Ph. Chomaz, and G. de France, Phys. Rev. Lett. **86**, 2971 (2001).

[42] J. A. Maruhn, P.-G. Reinhard, P. D. Stevenson, and M. R. Strayer, Phys. Rev. C **74**, 027601 (2006).

[43] K. Washiyama and D. Lacroix, Phys. Rev. C **78**, 024610 (2008).

[44] L. Guo and T. Nakatsukasa, Eur. Phys. J. Web Conf. **38**, 09003 (2012).

[45] C. Golabek and C. Simenel, Phys. Rev. Lett. **103**, 042701 (2009).

[46] D. J. Kedziora and C. Simenel, Phys. Rev. C **81**, 044613 (2010).

[47] T. Skyrme, Philos. Mag. **1**, 1043 (1956).

[48] P. Hoodbhoy and J. W. Negele, Nucl. Phys. A **288**, 23 (1977).

[49] P.-G. Reinhard and H. Flocard, Nucl. Phys. A **584**, 467 (1995).

[50] E. Chabanat, P. Bonche, P. Haensel, J. Meyer, and R. Schaeffer, Nucl. Phys. A **635**, 231 (1998).

[51] Y. M. Engel, D. M. Brink, K. Goeke, S. J. Krieger, and D. Vautherin, Nucl. Phys. A **249**, 215 (1975).

[52] J. Dobaczewski and J. Dudek, Phys. Rev. C **52**, 1827 (1995).

[53] K. H. Kim, T. Otsuka, and P. Bonche, J. Phys. G **23**, 1267 (1997).

[54] M. Dasgupta, D. J. Hinde, N. Rowley, and A. M. Stefanini, Annu. Rev. Nucl. Part. Sci. **48**, 401 (1998).

[55] A. S. Umar and V. E. Oberacker, Phys. Rev. C **74**, 021601(R) (2006).

[56] A. S. Umar and V. E. Oberacker, Phys. Rev. C **74**, 024606 (2006).

[57] A. S. Umar and V. E. Oberacker, Eur. Phys. J. A **39**, 243 (2009).

[58] A. S. Umar, V. E. Oberacker, J. A. Maruhn, and P.-G. Reinhard, Phys. Rev. C **81**, 064607 (2010).

[59] R. Keser, A. S. Umar, and V. E. Oberacker, Phys. Rev. C **85**, 044606 (2012).

[60] A. S. Umar and V. E. Oberacker, Phys. Rev. C **77**, 064605 (2008).

[61] H. Spinka and H. Winkler, Nucl. Phys. A **233**, 456 (1976).

[62] J. S. Blair, Phys. Rev. **95**, 1218 (1954).

[63] D. L. Hill and J. A. Wheeler, Phys. Rev. **89**, 1102 (1953).

[64] S. Gary and C. Volant, Phys. Rev. C **25**, 1877 (1982).

[65] M. Evers, M. Dasgupta, D. J. Hinde, D. H. Luong, R. Rafiei, R. du Rietz, and C. Simenel, Phys. Rev. C **84**, 054614 (2011).

[66] A. S. Umar, V. E. Oberacker, and J. A. Maruhn, Eur. Phys. J. A **37**, 245 (2008).

[67] K. Washiyama, S. Ayik, and D. Lacroix, Phys. Rev. C **80**, 031602 (2009).

[68] C. Simenel, Phys. Rev. Lett. **105**, 192701 (2010).

[69] B. Yilmaz, S. Ayik, D. Lacroix, and K. Washiyama, Phys. Rev. C **83**, 064615 (2011).

[70] C. Simenel, D. J. Hinde, R. du Rietz, M. Dasgupta, M. Evers, C. J. Lin, D. H. Luong, and A. Wakhle, Phys. Lett. B **710**, 607 (2012).

[71] K. Sekizawa and K. Yabana, Phys. Rev. C **88**, 014614 (2013).

[72] R. Balian and M. Vénéroni, Phys. Lett. B **136**, 301 (1984).

[73] C. Simenel, Phys. Rev. Lett. **106**, 112502 (2011).

[74] M. Assié and D. Lacroix, Phys. Rev. Lett. **102**, 202501 (2009).

[75] K. Hagino and N. Takigawa, Prog. Theor. Phys. **128**, 1061 (2012).

[76] C. Simenel, Ph. Chomaz, and G. de France, Phys. Rev. Lett. **93**, 102701 (2004).

[77] C. Simenel, Ph. Chomaz, and G. de France, Phys. Rev. C **76**, 024609 (2007).

[78] V. E. Oberacker, A. S. Umar, J. A. Maruhn, and P.-G. Reinhard, Phys. Rev. C **85**, 034609 (2012).

[79] R. H. Spear, At. Data Nucl. Data Tables **42**, 55 (1989).

[80] K. Hagino, N. Takigawa, M. Dasgupta, D. J. Hinde, and J. R. Leigh, Phys. Rev. Lett. **79**, 2014 (1997).

[81] B. Avez, C. Simenel and Ph. Chomaz, Phys. Rev. C **78**, 044318 (2008).

[82] C. Simenel and Ph. Chomaz, Phys. Rev. C **68**, 024302 (2003).

[83] A. S. Umar and V. E. Oberacker, Phys. Rev. C **71**, 034314 (2005).

[84] J. A. Maruhn, P. G. Reinhard, P. D. Stevenson, J. R. Stone, and M. R. Strayer, Phys. Rev. C **71**, 064328 (2005)

[85] P.-G. Reinhard, L. Guo, and J. A. Maruhn, Eur. Phys. J. A **32**, 19 (2007).

[86] C. Simenel and Ph. Chomaz, Phys. Rev. C **80**, 064309 (2009).

[87] S. Fracasso, E. B. Suckling, and P. D. Stevenson, Phys. Rev. C **86**, 044303 (2012).

[88] B. Avez and C. Simenel, Eur. Phys. J. A **49**, 76 (2013).

[89] K. Hagino, N. Rowley, and A. T. Kruppa, Comput. Phys. Commun. **123**, 143 (1999).

[90] L. C. Chamon *et al.*, Phys. Rev. C **66**, 014610 (2002).

[91] R. Y. Cusson, P.-G. Reinhard, M. R. Strayer, J. A. Maruhn, and W. Greiner, Z. Phys. A **320**, 475 (1985).

[92] K. Hagino and Y. Watanabe, Phys. Rev. C **76**, 021601(R) (2007).